Submitted version

BALLISTIC-ELECTRON-EMISSION MICROSCOPY OF STRAIN NON-UNIFORMITIES IN $Si_{1-x}Ge_x$/Si STRUCTURES

L. D. Bell, W. J. Kaiser, S. J. Manion, A. M. Milliken, R. W. Fathauer, and W. T. Pike

Center for Space Microelectronics Technology
Jet Propulsion Laboratory
California Institute of Technology
Pasadena, CA 91109

Ballistic-electron-emission microscopy (BEEM) is used to probe local conduction-band structure in strained $Si_{1-x}Ge_x$ layers of pseudomorphic $Si_{1-x}Ge_x$/Si heterostructures. The strain variation produced by a roughened $Si_{1-x}Ge_x$ surface is seen as a variation of splitting between thresholds in BEEM spectroscopy. This splitting is directly related to the strain-induced conduction-band splitting in the $Si_{1-x}Ge_x$ layer, enabling BEEM to directly measure local strain variations. Elasticity calculations for a roughened $Si_{1-x}Ge_x$ surface predict variations in strain that are consistent with BEEM observations. For the case of a smooth $Si_{1-x}Ge_x$ surface, a uniform conduction-band splitting is observed which is in good agreement with calculations.

PACS Numbers: 73.30.+y, 71.70.Ej, 61, 16.Ch, 73.40.Ns

I. Introduction.

The growth capability for strained $Si_{1-x}Ge_x$/Si heterostructures has advanced in recent years, allowing production of high-quality layers with lower densities of defects and of greater thicknesses and alloy fractions. 'I'he pseudomorphic $Si_{1-x}Ge_x$/Si system is a candidate for novel devices such as heterojunction bipolar transistors, [1] providing high mobility and device speed, coupled with the very desirable characteristic of integration with existing Si technology. Factors limiting device performance include the presence of defects and the roughness of interfaces with other materials. In order to adequately describe the performance of devices based on this material, fundamental aspects of $Si_{1-x}Ge_x$ electronic structure must be directly measured. This paper describes the application of ballistic-electron-emission microscopy[2] (BEEM) to an investigation of strain in metal/$Si_{1-x}Ge_x$/Si(1 00) structures.

Pseudomorphic $Si_{1-x}Ge_x$ layers maybe grown on Si substrates provided the layers remain thinner than the critical thickness for the introduction of misfit dislocations. The $Si_{1-x}Ge_x$ lattice constant is larger than that of Si; therefore, epitaxial growth of thin layers of $Si_{1-x}Ge_x$ on Si induces biaxial compressive strain in the plane of the layer. Since the Poisson ratio for $Si_{1-x}Ge_x$ is positive, off-diagonal elements of the elasticity tensor produce tensile strain normal to the layer. The presence of strain modifies the $Si_{1-x}Ge_x$ band structure, The four strain-equivalent conduction-band minima in the layer plane are lowered in energy, while the two minima normal to the plane are raised in energy. This conduction-band splitting has been calculated as a function of alloy fraction,[3,4] and has recently been measured by electron-energy-loss spectroscopy for a thin $Si_{1-x}Ge_x$ quantum well.[5] In addition, the light- and heavy-hole valence. bands are split at the zone center by strain.

BEEM is based on scanning tunneling microscopy[6] (STM). The STM tip is used to inject hot carriers into the sample structure, which normally consists of a metal base layer and a semiconductor collector. Currents entering the base and collector are measured separately. By performing measurements as a function of tunnel voltage, a spectroscopy of carrier transport through the structure may be performed. Metal/ semiconductor interface characteristics[7,8] and aspects of transport through the metal or semiconductor[9-12] have been investigated by BEEM in the past, in a wide range of materials systems. Since the injection is by vacuum tunneling from an STM tip, spatial resolution of the technique is normally very high (on the order of a few nanometers or less).

Since the two sets of strain-split conduction-band minima in $Si_{1-x}Ge_x$ lie at different points in the interface Brillouin zone, it is expected that the onset of transmission into the two sets of states will produce a BEEM spectrum with two thresholds. The relative intensities of the two contributions will be determined at each point by the electron momentum distribution at the metal/semiconductor interface. This depends to a large extent on the degree of scattering the electrons undergo during transport through the metal layer. In the case of Au/GaAs, BEEM spectra always show thresholds due to the off-axis (L and X) minima, indicating that substantial broadening of the electron distribution occurs during traversal of the Au.

The growth and preparation of the samples for BEEM have been described in detail elsewhere.[13] $Si_{1-x}Ge_x$ layers were grown on Si(1 00) substrates by molecular-beam epitaxy (MBE). These were undoped and nominally pseudomorphically strained (well below the critical thickness). The layers were nominally 50 nm thick; alloy fractions of x=O. 18 and 0.25 were grown. The wafers were diced and prepared for BEEM by evaporation of either Au layers or Ag layers capped by Au, BEEM measurements were

performed in a glove-box purged by dry nitrogen, at both room temperature and 77K.

II. Experimental Results.

A series of samples for BEEM was fabricated consisting of 10 nm of Au on $Si_{1-x}Ge_x/Si$. In contrast to Au/Si, which yield BEEM spectra exhibiting a single threshold, the $Au/Si_{1-x}Ge_x/Si$ samples usually produced a two-threshold spectrum. These thresholds are due to the onset of transmission into the separate sets of conduction band minima which are split by strain. The value of the splitting, however, was unexpectedly found to vary from point to point across the sample, with values ranging from near zero to nearly twice the calculated value. An example of each of these extreme cases is shown in Fig. 1.

The large variation in conduction-band splitting observed by BEEM spectroscopy clearly indicates heterogeneous strain in the $Si_{1-x}Ge_x$ layer. There are several possibilities to consider in accounting for this variation. A spatial variation in alloy fraction within the $Si_{1-x}Ge_x$ layer would produce regions of varying lattice constant and induced strain. This would imply that regions where BEEM measurements produce single threshold spectra correspond to areas where the alloy fraction is nearly zero. In order to test this possibility, all individual spectra were fitted to a two-threshold model, and the cases in which these thresholds converged to a single value were compiled, and the fitted thresholds for a given nominal alloy fraction and temperature were averaged. The results are given in Fig. 2. The steady decrease of Schottky barrier height with increasing nominal alloy fraction argues against local alloy fraction variation as a cause of strain heterogeneity. If such a situation existed, all of the compiled spectra would represent areas where local alloy fractions were nearly zero and would yield a barrier height that is independent of nominal alloy fraction.

Another possible cause of strain variation is surface roughness of the as-grown strained layer. A periodic surface roughness has been observed for certain growth conditions by other workers.[14,15] With a rough surface, strain is generally decreased in high areas and enhanced in low areas. The nature of the $Si_{1-x}Ge_x$ surface used in this work was investigated by cross-sectional transmission electron microscopy (TEM). A TEM image of the surface of a $Si_{.75}Ge_{.25}$ sample is shown in Fig. 3(a). It is apparent that the surface is smooth, with no evidence of large scale roughness such as that seen in ref. 15.

Although the as-grown $Si_{1-x}Ge_x$ surface is smooth, the presence of the Au may modify the $Si_{1-x}Ge_x$ surface. This possibility was also investigated. TEM was performed on a $Au/Si_{.82}Ge_{.18}/Si$ sample, and the result is shown in Fig, 3(b). In contrast to the previous case of bare $Si_{1-x}Ge_x$, large-scale roughness is seen for the $Si_{1-x}Ge_x$ surface in the presence of Au. This roughness has an amplitude on the order of 3 nm, and on a length scale of order 10 to 50 nm.

The interaction between Au and $Si_{1-x}Ge_x$ has a dramatic effect on the interface between the two materials. A comparison was made with another metal that did not produce this roughening. Ag was found to be such a metal. A new series of samples was fabricated which consisted of 8 nm of Ag deposited onto the $Si_{1-x}Ge_x$ surface. An additional 8 nm of Au was then evaporated to protect the surface from oxidation during BEEM measurements. TEM imaging demonstrates that the $Ag/Si_{1-x}Ge_x$ interface remains smooth, as shown in Fig. 3(c).

Since Ag does not roughen the $Si_{1-x}Ge_x$ surface, BEEM spectroscopy should not exhibit the strain variation apparent in the Au case. As expected, BEEM spectra of the $Ag/Si_{1-x}Ge_x/Si$ system always showed two thresholds. Moreover, the separation of these

thresholds was uniform and in good agreement with calculations. The results are shown in Fig. 4. The calculated splitting, shown by a line, will be discussed later. These experiments clearly indicate a correlation between the variation in strain observed by BEEM and $Si_{1-x}Ge_x$ surface roughening.

The strain variation observed for $Au/Si_{1-x}Ge_x/Si$ structures was also observed in systems which onl y involved a Au/Si interface. MBE was used to grow a thick (300 nm) $Si_{.75}Ge_{.25}$ layer on a Si substrate. This thickness substantially exceeds the critical thickness for strain relaxation. A 50 nrn strained Si layer was then grown on the relaxed $Si_{.75}Ge_{.25}$. 10 nm of Au completed the sample for BEEM. In this case, the in-plane conduction-band minima are raised in energy, and the out-o f-plane minima are lowered, but the magnitude of the splitting for strained Si on relaxed $Si_{.75}Ge_{.25}$. is the same as for strained $Si_{.75}Ge_{.25}$.

BEEM spectroscopy of these structures revealed strain variation in the same range as did measurements of the previous $Au/Si_{1-x}Ge_x$ samples. In both cases, the observed conduction-band splitting varies from near zero to nearly twice the calculated splitting. BEEM spectra were also obtained for $Au/Ag/Si/Si_{1-x}Ge_x$(relaxed); in this case, uniform splittings were observed, just as with strained $Si_{1-x}Ge_x$ samples incorporating Ag. For comparison to the prior data, the splitting value for these samples is included on Fig. 4.

The deposition of Au onto Si is known to produce a strong interdiffusion, even at room temperature and below. [16] Most work has been done on Si(1 11), but Au/Si(1 00) has also been studied. [17] A similar reaction may be expected on $Si_{1-x}Ge_x$ of lower alloy fractions. Although the detailed mechanism is not yet well understood, [18] the Au has been found to induce breaking of the Si-Si bonds, and intermediate alloys have been observed to form[19-21] which are metastable. [19] The Si atoms in the alloy are therefore easily

released and diffuse to the Au surface; indeed, the diffusion rate of Si through Au is surprisingly high.[21] The diffusion can be non-uniform, depending on trace contamination remaining at the Au/Si interface,[19] and perhaps on Au crystallite orientation. In contrast, Ag is notably unreactive with Si; intermixing and silicide formation are minimal[22-24], and Si surface reconstructions have been observed to persist even under thick Ag layers.[25] Ag/Si has recently been used as a "model" Schottky barrier system.[26] As shown by the BEEM and TEM results, this diffusion process leads top a roughened interface, producing heterogeneity in the strain of the layer and a corresponding variation in BEEM threshold splitting.

Pidduck et al.[15] have discussed a spontaneous relaxation of the bare $Si_{1-x}Ge_x$ surface for certain growth parameters. As a result of this surface relaxation, strain is decreased in the neighborhood of the peaks and enhanced in the troughs. Although the roughness observed in the case of $Au/Si_{1-x}Ge_x$ is of a different nature, involving removal of material by diffusion, the same qualitative arguments for variation of strain apply. Partial removal of lateral constraint around high areas allows partial relaxation of strain in these regions, and this relaxation induces strain enhancement in the low areas.

III. Elastic Modeling: The Effect of Surface Roughness.

It remains to be shown that the degree of roughness observed by TEM is consistent with the range of conduction-band splittings derived from BEEM data. Since the strain variation induced by the surface roughness is of arbitrary magnitude and direction, it was necessary to use numerical methods for this calculation. The lattice-matched $Si_{1-x}Ge_x/Si$ system is described well by elasticity theory;[3] therefore, a finite-element implementation of elasticity was chosen to model the problem. The derived strains in the layer were then used to calculate conduction-band positions and splittings.

The equilibrium strain configuration of the $Si_{1-x}Ge_x$ layer was determined by the solution to a linear stress-strain relationship using a two-dimensional finite-element system, An array was used to represent the $Si_{1-x}Ge_x$ layer of our samples, which was nominally 50 nm thick, Periodic boundary conditions were used laterally, with the last node of a row mathematically connected to the first node of the same row. A rigid Si substrate lattice was used to fix the bottom row. Since the degree of roughness was determined by reference to Fig 3(b), initial strain in the layer was chosen to be that appropriate for $Si_{0.82}Ge_{0.18}$ lattice-matched to Si. Elastic constants for Si and Ge were linearly interpolated to arrive at constants for the alloy. Strain in the third dimension was fixed at a constant value.

Table I lists the lattice constants *a* and elastic constants for Si and Ge. 18 The derived Poisson ratio v is also shown. Values for $Si_{0.82}Ge_{0.18}$ are linear interpolations.

TABLE I

	Si	Ge	$Si_{0.82}Ge_{0.18}$
a (m)	0.5431	0.5658	0.5472
c_{11} (Mbar)	1.656	1.285	1.589
c_{12} (Mbar)	0.639	0.483	0.611
C44 (Mbar)	0.795	0.680	0.774
$\nu=c_{12}/(c_{11}+c_{12})$	0.278	0.273	0.278

The lattice constants in Table I yield a bulk value for uniaxial strain of

$$e_{xx} = (a_{Si} - a_{SiGe}) / a_{SiGe} = -0.749\% \quad (1)$$

in the plane of the $Si_{0.82}Ge_{0.18}$ layer, with the sign indicating compressive strain. Strain in the third dimension (normal to the grid) was maintained at $e_{yy} = -0.749\%$. Resulting extension in the direction normal to the plane of the layer is

$$e_{zz} = -2 \frac{c_{12}}{c_{11}} e_{xx} = 0.576’?4.. \quad (2)$$

The array was initialized using these values.

In order to calculate band positions from the strains, hydrostatic, uniaxial, and chemical contributions are considered. There have been several treatments of band shifts in the strained $Si_{1-x}Ge_x/Si$ syst em.[3,4] The procedure used here has been outlined by van de Wane and Martin.[4] The positions of the strained $Si_{1-x}Ge_x$ bands relative to the Si valence bands may be derived via four general steps for the case of strain and/or chemistry variations.

First of all, the $Si_{1-x}Ge_x$ valence band may be aligned with the Si valence band using the interpolation

$$E_{v,av} = E_v + 0.54X , \quad (3)$$

where $E_{v,av}$ is the energy of the weighted average of the strain-split $Si_{1-x}Ge_x$ valence-band maxima and E_v is the energy of the Si valence band maximum, Calculations by van de Wane and Martin[4] indicate that this interpolation is nearly independent of orientation and

strain conditions in the layer.

Next, the weighted average of the $Si_{1-x}Ge_x$ conduction-band minima is located relative to the $Si_{1-x}Ge_x$ valence-band maxima using experimental (unstrained) alloy band-gap data. The data of Braunstein et al.[28] was used for this purpose. The values derived from that work were shifted upwards by 0.025 eV to reproduce the measured band gap for Si of 1.12 eV at 300K.

The resulting conduction-band position is then corrected for strain-induced hydrostatic shifts using the appropriate deformation potential. This deformation potential is denoted by $(\Xi_d + \frac{1}{3}\Xi_u - a)$, and the energy shift of the conduction bands relative to the valence bands is given by

$$E_h = (\Xi_d + \tfrac{1}{3}\Xi_u - a)(\vec{1}:\ddot{e}) = (\Xi_d + \tfrac{1}{3}\Xi_u - a)(e_{xx} + e_{yy} + e_{zz}). \quad (4)$$

Finally, the conduction band splitting due to uniaxial strain is used to position the individual conduction bands relative to the weighted average. The deformation potential for this contribution is Ξ_u, and the energy shift for a given conduction-band minimum is

$$E_u^i = \Xi_u\left[\{\hat{a}_i\hat{a}_i\}:\ddot{e} - \tfrac{1}{3}(\vec{1}:\ddot{e})\right], \quad (5)$$

where $\hat{a}_i$ is the unit vector in the direction of the ith conduction band minimum, and $\{\hat{a}_i\hat{a}_i\}$ denotes a dyadic product. Thus,

$$\{\hat{a}_i\ \hat{a}_i\}:\ddot{e} = e_{xx}, \qquad \hat{a}_i = [100] \text{ or } [\text{Too}] \tag{6a}$$

$$\{\hat{a}_i\ \hat{a}_i\}:\ddot{e} = e_{yy}, \qquad \hat{a}_i = [010] \text{ or } [0\bar{1}0] \tag{6b}$$

$$\{\hat{a}_i\ \hat{a}_i\}:\ddot{e} = e_{zz}, \qquad \hat{a}_i = [001] \text{ or } [00\bar{1}] \tag{6c}$$

and

$$E_u^x = \Xi_u\left[+\tfrac{2}{3}e_{xx} - \tfrac{1}{3}e_{yy} - \tfrac{1}{3}e_{zz}\right] \tag{7a}$$

$$E_u^y = \Xi_u\left[-\tfrac{1}{3}e_{xx} + \tfrac{2}{3}e_{yy} - \tfrac{1}{3}e_{zz}\right] \tag{7b}$$

$$E_u^z = \Xi_u\left[-\tfrac{1}{3}e_{xx} - \tfrac{1}{3}e_{yy} + \tfrac{2}{3}e_{zz}\right]. \tag{7c}$$

Energy differences between minima are given by

$$E_u^z - E_u^x = \Xi_u[+e_{zz} - e_{xx}] \tag{8a}$$

$$E_u^z - E_u^y = \Xi_u[+e_{zz} - e_{yy}]\ . \tag{8b}$$

For uniform in-plane compressive strain of the layer (e_{xx} and e_{yy} negative) energies of [00”] minima will in general be raised, and the energies of [100] and [010] minima will be lowered,

It is important to note that, since the observed variation in strain is attributed to surface roughness, all three components of strain will in general be different. This would produce a BEEM spectrum which exhibits three separate thresholds. In practice, however, it is more difficult to reliably resolve three thresholds than two. In order to clearly distinguish the three thresholds, it is necessary to have large strain and also to have the intermediate threshold roughly equidistant between the other two. Since this is a relatively uncommon situation, we have parameterized the spectra in this work with two-

threshold fits. While this may underestimate the separation between the highest and lowest of three thresholds, it is unlikely to overestimate.

The deformation potentials for Si and Ge are given in Table 11.[4] Also shown are linear interpolations for $Si_{0.82}Ge_{0.18}$. Deformation potentials listed are those for the A minima; these are used for the alloy interpolation, since for x=0. 18 this minimum is lowest in energy for all values of strain.[4] For uniformly strained $Si_{0.82}Ge_{0.18}$, Eq. 8 and the interpolated value of Ξ_u yield a bulk value for conduction-band splitting of 122,5 meV. This is also the source of the calculated splitting shown in Fig. 4.

TABLE 11

	Si	Ge	$Si_{0.82}Ge_{0.18}$
Ξ_u (eV)	9.16	9.42	9.21
$(\Xi_d + \frac{1}{3}\Xi_u - a)$ (eV)	1.72	1.31	1.65

The initial calculations for the roughened metal/semiconductor interface were performed using a sinusoidal profile for the $Si_{1-x}Ge_x$ surface. The amplitude and period were selected to approximate the profile observed by TEM. Layer thickness as determined from cross-sectional TEM was approximately 56 nm; amplitude and period, A =2.05 nmand P= 56 nm, respectively, were assigned for the sinusoidal profile. Other amplitude and period values were investigated as well.

Figures 5(a) and 5(b) show this sinusoidal surface for the above parameters. Using

this profile, the elasticity model was used to obtain components of strain at the surface. These components e_{xx} and e_{zz} are plotted in Fig. 6. Also shown for reference are the bulk values. Note that both components of strain are distinctly non-sinusoidal and are not symmetric about the bulk values. Figure 5(c) shows the conduction-band splitting along the surface, derived from Eq. 8 using the calculated surface strains. Also shown is the bulk value of splitting in the absence of surface roughness. The variation in splitting is from 0.095 eV to 0.144 eV, or from 78% to 118% of the bulk value.

Since a two-dimensional model is used for the strain calculation, it is limited to the imposition of a constant strain in the third dimension. However, the roughness at the $Au/Si_{1-x}Ge_x$ interface extends to both lateral dimensions, and the TEM micrograph of Fig. 3(b) may be thought to represent the typical roughness in an arbitrary lateral direction. One aim of these calculations is to derive an expected maximum and minimum splitting for the observed roughness. This can be estimated by varying the constant strain e_{yy} and calculating new maximum and minimum splittings. e_{yy} was varied between the maximum and minimum values of e_{xx}. This procedure slightly increased the expected maximum splitting value to O,151 eV and slightly decreased the minimum to 0.087 eV; these corrected values are also indicated in Fig, 5(c).

In general, the maximum and minimum strains at the surface depend only on the amplitude-to-period ratio (A/P) of the sinusoidal roughness, as long as the strain distortion imposed by the roughness decays sufficiently quickly with depth. In practice this seems to be true for P less than the layer thickness. Several A/P values were modeled, and the results for the maximum and minimum conduction-band splittings are plotted in Fig. 7, corrected as described above to estimate the effect of the two-dimensional nature of the surface roughness. It can be seen that the maximum and minimum are not symmetric about the bulk splitting value, a characteristic that is also apparent in Figs. 5 and 6. This is

reasonable, since the lateral constraints of elements at the bottom of surface troughs are not directly affected by roughness, but only indirectly by the secondary effect of the relaxation of high areas.

Having investigated the variation in splitting due to a simple form of roughness, the actual surface profile shown in Fig, 3(b) was next used for more specific calculations. A 200 nm section of this surface was used in the elasticity model, This portion is shown in Figs. 8(a) and 8(b), The splitting across the surface due to this one-dimensional profile, derived from calculated strains, is reproduced in Fig. 8(c). In this case also the expected minimum and maximum splittings for an equivalent roughness in the third dimension are estimated in the same way as for the sinusoidal case, and are indicated in Fig. 8(c). These corrected values range from 0.084 eV to 0.170 eV.

In addition to characterizing the strain distortion across the surface of the $Si_{1-x}Ge_x$ layer, it is also important to determine the penetration of the distortion into the layer. Since strains are calculated everywhere within the layer, the conduction-band splitting may be determined away from the surface as well, Two vertical cuts through the grid were chosen, at the points of minimum and maximum surface splitting. As shown in Fig 8(c), maximum conduction-band splitting occurs at 103 nm, and minimum splitting is at 71 nm. Conduction-band splittings along these cuts are plotted in Fig, 9. Due to the high spatial frequencies present in the surface topography, the perturbation in the splitting produced by the surface roughness decays relatively quickly with depth. The calculated values converge to the bulk value of 122.5 meV as the SiGe/Si interface is approached.

Band positions were also determined along these cuts from the surface to the SiGe/Si interface. Initial unstrained $Si_{1-x}Ge_x$ band gap and $Si_{1-x}Ge_x$/Si valence band offset for x=O. 18 were set using ref. 28 and Eq. 3, respectively. The position of the Fermi

level at the surface was determined from BEEM measurements of Schottky barrier height for Au/$Si_{1-x}Ge_x$/Si structures, using only the unstrained (zero-splitting) data. Poisson's equation was then solved using HETMOD[29] and the known doping levels for the structure. Conduction-band strain shifts (hydrostatic and uniaxial) were added using Eqs. 4 and 5 and the calculated strains. These shifts were applied relative to the conduction-band minimum of unstrained $Si_{1-x}Ge_x$. This was also done at the surface, which assumes that the pinning position relative to the weighted average of the conduction band minima is not strongly affected by strain.[30]

The derived conduction-band profiles for the vertical cut through the point of maximum surface splitting (at the 103 nm mark in Fig 8(c)) are shown in Fig. 10(a). Strain shifts of the valence bands have not been included in this Figure. The strain gradient near the surface is large enough that the splitting actually causes the lower conduction band to maximize below the surface. Since a BEEM threshold is sensitive to the highest point in the conduction-band minimum profile (in the absence of tunneling),[31] BEEM threshold separation will in such a case slightly underestimate the true band splitting at the surface. It can be seen that the strain distortion produced by surface roughness has appreciable effect on the band splitting only within about 10 nm of the surface.

Conduction-band profiles below the point of minimum surface splitting (at x = 71 nm in Fig 8(c)) are plotted in Fig. 10(b). Similar behavior is observed for this case, with the bulk of the strain distortion confined within 10 nm of the surface. As Figs. 10(a) and 10(b) indicate, the full range of variation in surface conduction-band splitting for very short period roughness may be underestimated by BEEM spectroscopy. This occurs due to the fact that short-period surface corrugation produces a strain distortion that penetrates only a short distance into the layer. Figure 10(a) illustrates a case in which the

energy of the lower conduction band maximum at the surface may be overestimated; the energy of the upper conduction band maximum may be underestimated, due to carrier tunneling through a very narrow depletion region, The total measured band splitting is therefore less than the actual surface value. Similarly, Fig, 10(b) suggests that the opposite situation may also occur, where the energy of the lower conduction band maximum at the surface may be underestimated (due to tunneling), and the energy of the upper conduction band maximum may be overestimated. The measured band splitting for such a case may thus be greater than the actual value at the surface.

IV. Summary.

In conclusion, strain-induced conduction-band splittings in $Si_{1-x}Ge_x$ layers have been measured by BEEM. $Ag/Si_{1-x}Ge_x/Si$ structures exhibit spatially uniform splitting, with values that agree well with calculations. $Au/Si_{1-x}Ge_x/Si$ structures reveal spatially heterogeneous strain splitting, with values ranging from near zero to approximately twice the calculated value. This variation is explained in terms of $Si_{1-x}Ge_x$ roughening by Au-Si interdiffision at the $Au/Si_{1-x}Ge_x$ interface. TEM clearly shows the nature of this roughness, which is not present in the heterostructures incorporating Ag. Elasticity calculations for surface roughness on a strained $Si_{1-x}Ge_x$ layer produce a strain variation of more than a factor of two. A more sophisticated model should be used to assess the agreement with the experimental variation more precisely; however, the simple model used here provides encouraging agreement with the conduction-band splitting variations observed by BEEM spectroscopy. Thus the variation in observed splittings is attributed to the diffusion-induced roughening at the $Au/Si_{1-x}Ge_x$ interface. Finall y, examples were given for cases of extreme strain non-uniformity where BEEM measures a reduced range of conduction-band splittings.

The authors wish to acknowledge valuable discussions with L. A. Branagan. The research described in this paper was performed by the Center for Space Microelectronics Technology, Jet Propulsion Laboratory, California Institute of Technology, and was jointly sponsored by the Office of Naval Research and the Ballistic Missile Defense Organization / Innovative Science and Technology Office through an agreement with the National Aeronautics and Space Administration (NASA).

REFERENCES

1. S. C. Jain and W. Hayes, Semicond. Sci. Technol. 6, 547 (1991).
2. W. J. Kaiser and L. D. Bell, Phys. Rev. Lett. 60, 1406 (1988); L. D. Bell and W. J. Kaiser, Phys. Rev. Lett. **61,2368 (1988).**
3. R, People, Phys. Rev. B 32, 1405 (1985).
4. C. G. Van de Wane and R. M. Martin, Phys. Rev. B 34, 5621 (1986).
5. P. E. Batson and J. F. Morar, Phys. Rev. Lett. 71, 609 (1993).
6. G. Binnig, H. Rohrer, Ch. Gerber, and E. Weibel, Phys. Rev. Lett. 49,57 (1982).
7. A. Femandez, H. D. Hallen, T. Huang, R. A. Buhrman, and J. Silcox, J. Vat. Sci. Technol. B 9,590 (1991).
8. M. Prietsch and R. Ludeke, Phys. Rev. Lett. 66,2511 (1991).
9. L. D. Bell, M. H. Hecht, W. J. Kaiser, and L. C. Davis, Phys. Rev. Lett. 64, 2679 (1990).
10. A. M. Milliken, S. J. Manion, W. J. Kaiser, L. I). Bell, and M. H, Hecht, Phys. Rev. B 46, 12826 (1992).
11. R. Ludeke, Phys. Rev. Lett. 70,214 (1993).
12. A, Bauer, M, T. Cuberes, M. Prietsch, and G. Kaindl, Phys. Rev. Lett. 71, 149 (1993).
13, L. D. Bell, A. M. Milliken, S. J. Mankm, W. J. Kaiser, R. W. Fathauer, and W. T. Pike, Phys. Rev. B 50, 8082 (1994).
14. A. G. Cullis, D. J. Robbins, A. J. Pidduck, and P. W. Smith, J. Cryst. Growth 123, 333 (1992).
15. A, J. Pidduck, D. J. Robbins, A. G. Cullis, W. Y. Leong, and A, M, Pitt, Thin Solid Films 222, 78 (1992).
16. S. L. Molodtsov, C. Laubschat, A. M. Shikin, and V. K. Adarnchuk, Surf Sci. 269/270, 988 (1 992).

17. M. Hanbucken, Z. Imam, J. J. Metois, and G. LeLay, Surf. Sci. 162, 628 (1985).
18. B. Lamontagne, E. Sacher, and M. R. Wertheimer, Appl. Surf Sci. 78, 399(1994).
19. Z, Ma and L. H. Allen, Phys. Rev. B 48, 15484 (1993).
20. P. Perfetti, S. Nannarone, F. Patella, C. Quaresima, M. Capozi, A. Savoia, and G. Ottaviani, Phys. Rev. B 26, 1125 (1982).
21. L. Hultman, A. Robertsson, H. T. G. Hentzell, I. Engstrom, and P. A. Psaras, J. Appl. Phys. 62, 3647 (1987),
22. G. Raynerd, T. N. Doust, and J. A, Venables, Surf. Sci. 261,251 (1992),
23. G. P. Chambers and B. D, Sartwell, Surf. Int. Anal. 15, 126(1990).
24. K. Suganuma, S. Sugihara, and K. Okazaki, J. Mater. Sci. 29,4371 (1994).
25. H. Hong, R. D. Aburano, D. S. Lin, H. Chen, and T. C. Chiang, Phys. Rev. Lett. 68, 507 (1992),
26. R. F. Schmitsdorf, T. U. Kampen, and W. Monch, Surf Sci. 324,249 (1995).
27. ***CRC Handbook of Materials Science, Vol. III***, edited by Charles T. Lynch (CRC Press, Cleveland, 1975).
28. R. Braunstein, A. R. Moore, and F. Herman, Phys. Rev. 109,695 (1958)
29. HETMOD - Heterostructure Modeling Program Version 1.7- written by Alan C. Warren, Thomas J. Watson Research Center, Yorktown Heights, NY.
30. Since such a dependence of pinning position on strain depends on the specific interface model, some of which moreover do not provide prescriptions for including strain, this dependence cannot be compared unambiguously against theory. BEEM measurements in the present work indicate that Schottky barrier height, for a given alloy fraction, is largely independent of local strain.
31. L. D. Bell, S. J. Manion, M, H. Hecht, W. J. Kaiser, R. W. Fathauer, and A. M. Milliken, Phys. Rev. Lett. 48, 5712(1993).

FIGURES

1. (a) Experimental collector current (I_c) BEEM spectrum of for a Au/ $Si_{.75}Ge_{.25}$/ Si(1 00) heterostructure. Tunnel current for this spectrum was 3 nA. Also plotted are two theoretical spectra which have been fit to the data. The first (dashed line) fits only the low-voltage portion (V < 1. 1V) with a single threshold; the other fit (solid line) is over a larger range (to 1.6V) using a two-threshold model. The extracted thresholds for the two-threshold fit are separated by about 0.30 V. (b) BEEM I_c-V spectrum, taken on a sample identical to that in (a), showing only a single threshold. Tunnel current for this spectrum was 2 nA. Also plotted is a one-threshold fit to the data (solid line).

2. Dependence of Schottky barrier height (SBH) on Ge fraction x, compiled from all Au/$Si_{1-x}Ge_x$/Si BEEM spectra showing only a single threshold. Circles indicate 77K values, and squares indicate 295K values. Also shown are linear best-fits to the data.

3. Cross-sectional TEM images of $Si_{1-x}Ge_x$/Si structures. The SiGe/Si interface is out of the field of view in all three images. (a) Image of as-grown $Si_{.75}Ge_{.25}$ material. (b) Image of a $Si_{.82}Ge_{.18}$ sample with an evaporated Au layer of nominal thickness 10 nm. (c) Image of a $Si_{.82}Ge_{.18}$ sample with 8 nm of evaporated Ag, capped with 8 nrn of Au, (Non-uniform thinning during sample preparation is responsible for the dark area in the bottom right corner,)

4 Conduction-band splitting for Au/Ag/$Si_{1-x}Ge_x$/Si(1 00). The experimental points (circles) are derived from the fitted thresholds of the corresponding BEEM spectra. Also plotted (square) is the derived splitting for Au/Ag/Si(strained)/$Si_{1-x}Ge_x$ (relaxed) at x=.25. The calculated dependence (line) is from Eq. 8.

5. (a, b) Sinusoidal surface profile used in elasticity calculations. y=O corresponds to the $Si_{.82}Ge_{.18}/Si$ interface. (c) Calculated conduction-band splitting along this surface. The upper and lower dashed lines represent maximum and minimum values of strain after correction for roughness in two dimensions. The middle dashed line indicates the bulk splitting value.

6. (a) Sinusoidal surface profile used in elasticity calculations, as in Fig. 4(b). (b, c) Calculated strain components e_{xx} and e_{zz} along this surface. The dashed lines indicate the bulk values of the strain components.

7. Calculated maximum and minimum splittings at the surface of the $Si_{.82}Ge_{.18}$ layer as a function of amplitude/period ratio (A/P) of the sinusoidal surface roughness. These values have been corrected to estimate the effect of roughness in two dimensions, as described in the text. Also shown for reference is the bulk splitting value (dashed line).

8. (a, b) Experimental surface profile, a portion of which is shown in the TEM micrograph of Fig. 3(b). y=O corresponds to the $Si_{.82}Ge_{.18}/Si$ interface. (c) Calculated conduction-band splitting along this surface. As in Fig. 5(c), the upper and lower dashed lines represent maximum and minimum values of strain after correction for roughness in two dimensions, and the middle dashed line indicates the bulk splitting value.

9 Calculated conduction-band splitting along two vertical profiles (normal to the $Si_{.82}Ge_{.18}/Si$ interface) through the $Si_{.82}Ge_{.18}$ layer of Fig. 8. These two profiles are those through the points of (a) maximum and (b) minimum surface strain (lateral

distances x=103 nm and x=71 nm in Fig. 8, respectively).

10. Conduction-band positions calculated along directions normal to the $Si_{.82}Ge_{.18}/Si$ interface. (a) Profile through the point of maximum surface strain (x=103 nm in Fig, 8). (b) Profile through the point of minimum surface strain (%=71 nm in Fig, 8).

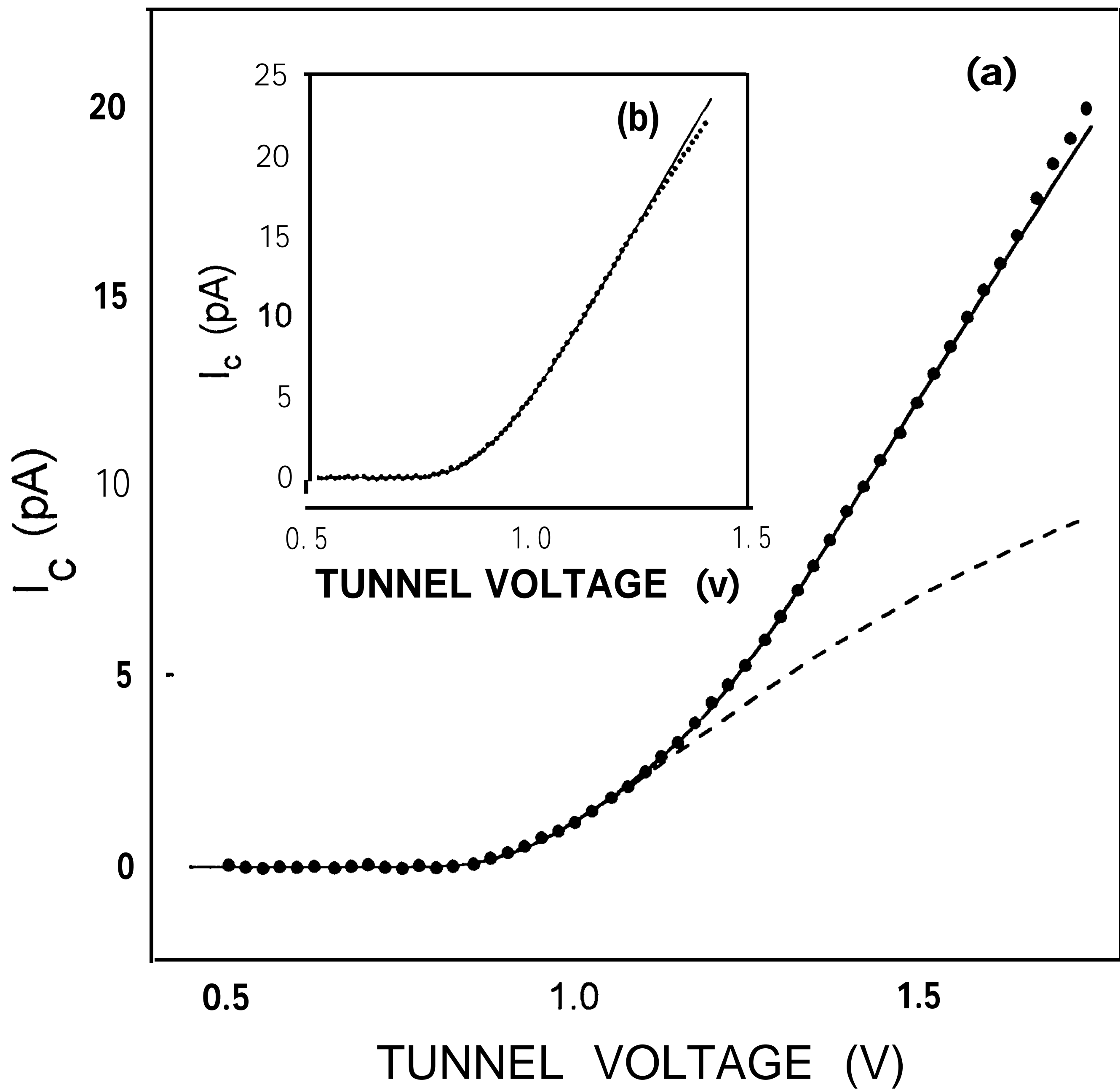

(a)
(b)
I_C (pA)
TUNNEL VOLTAGE (V)
TUNNEL VOLTAGE (v)
0
5
10
15
20
25
0.5
1.0
1.5

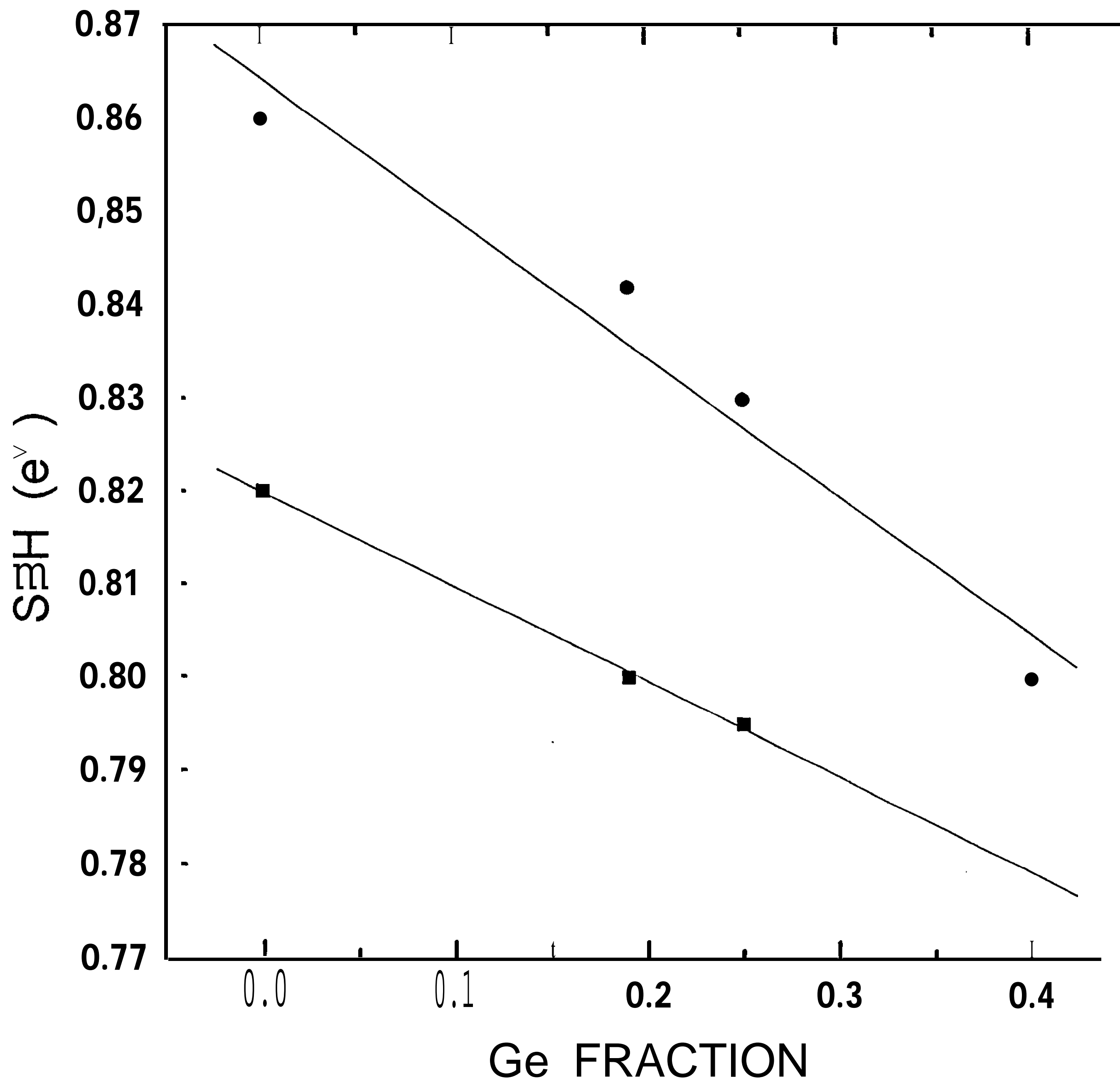

0.87
0.86
0,85
0.84
0.83
0.82
0.81
0.80
0.79
0.78
0.77
SEH (eV)
0.0
0.1
0.2
0.3
0.4
Ge FRACTION

a

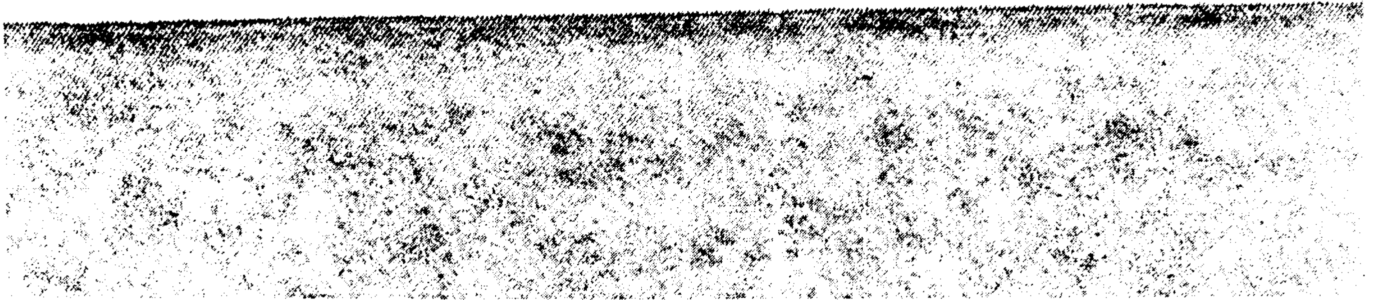

b

c

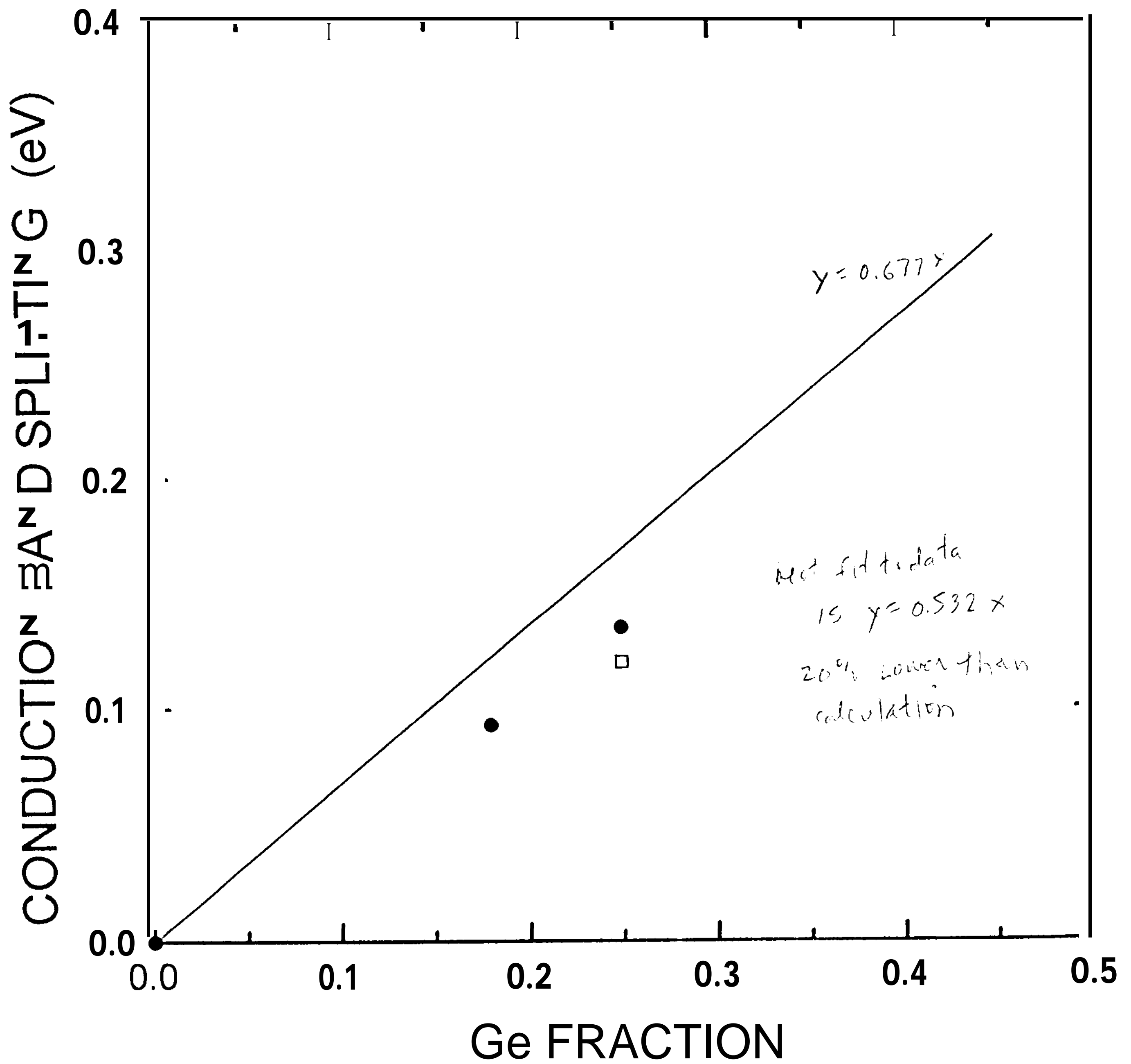
CONDUCTION BAND SPLITTING (eV)
0.0
0.1
0.2
0.3
0.4
0.0
0.1
0.2
0.3
0.4
0.5
Ge FRACTION
y = 0.677x
is y = 0.532 x
20% lower than
calculation

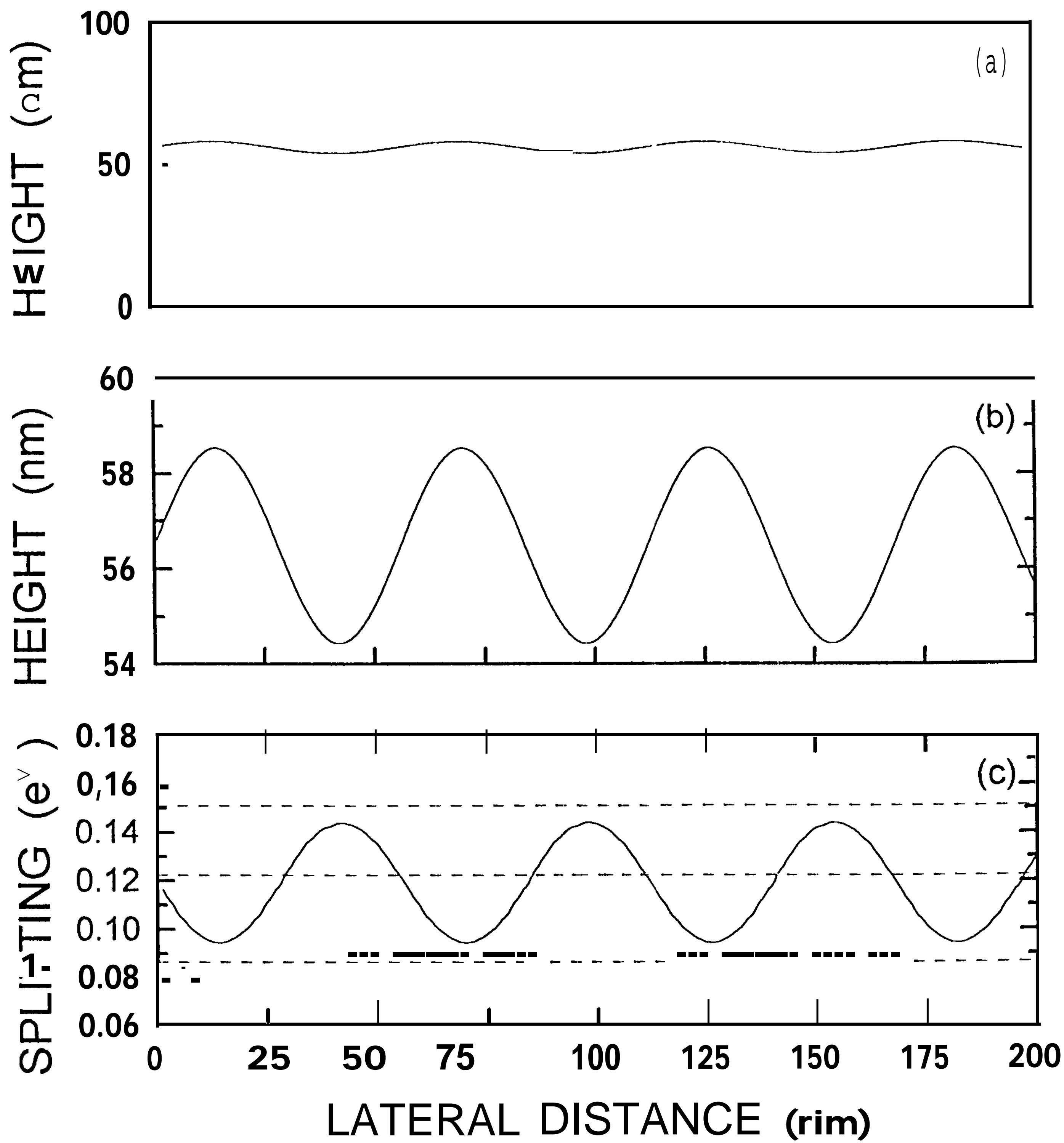

100
50
0
HEIGHT (nm)
(a)
60
58
56
54
HEIGHT (nm)
(b)
0.18
0,16
0.14
0.12
0.10
0.08
0.06
SPLITTING (eV)
(c)
0
25
50
75
100
125
150
175
200
LATERAL DISTANCE (nm)

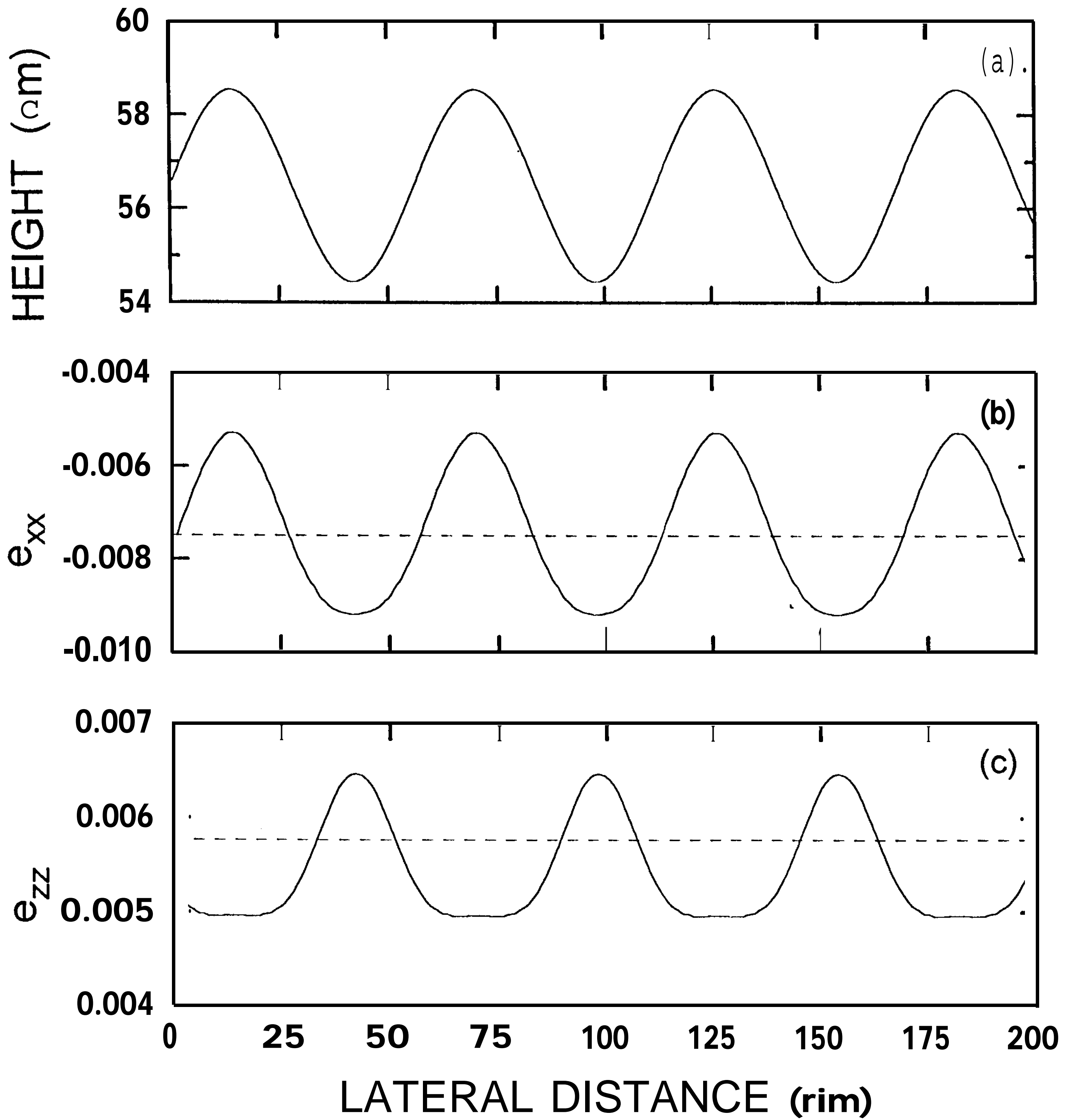

SiGe 17a

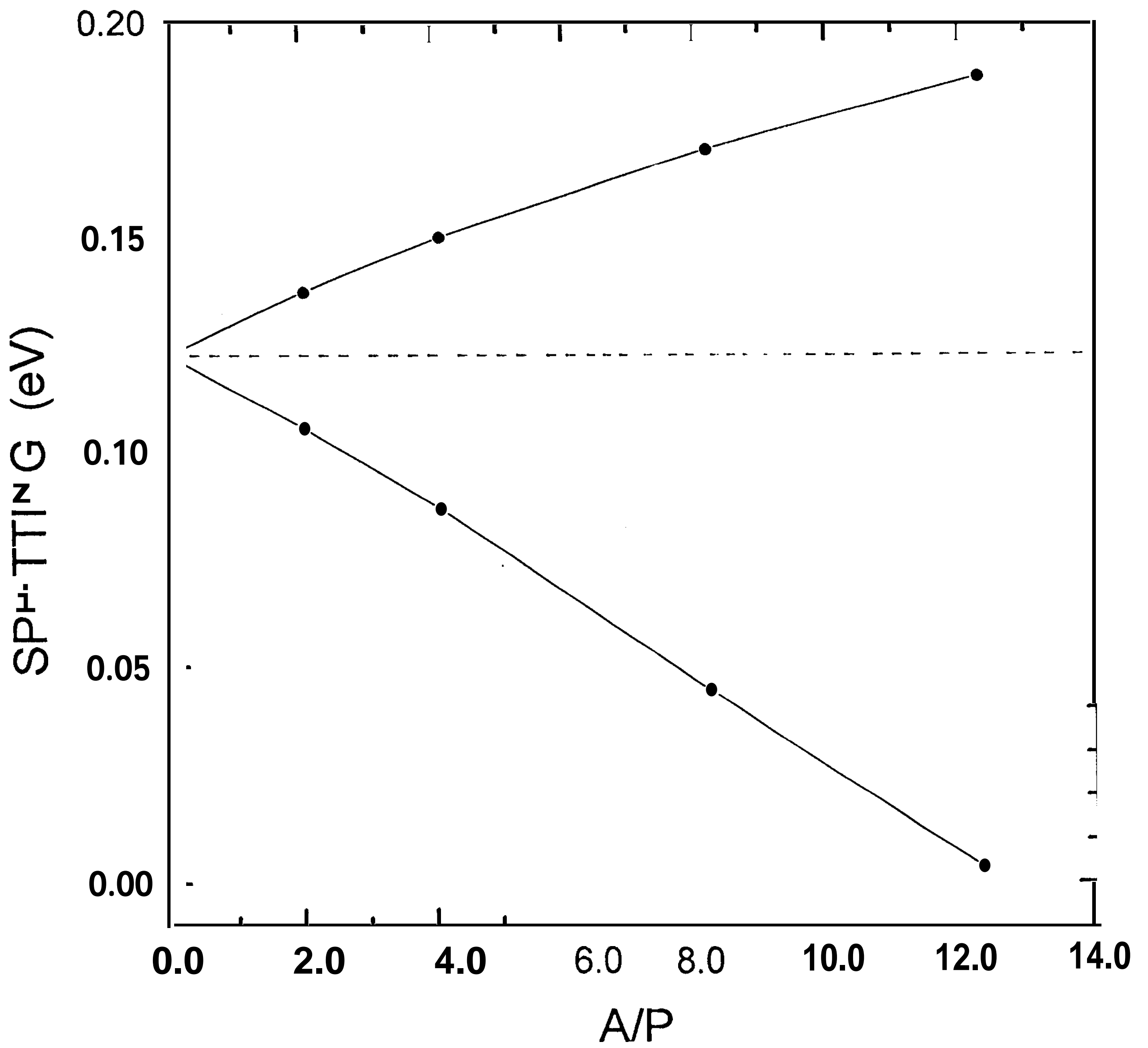
0.20
0.15
0.10
0.05
0.00
(eV)
0.0
2.0
4.0
6.0
8.0
10.0
12.0
14.0
A/P

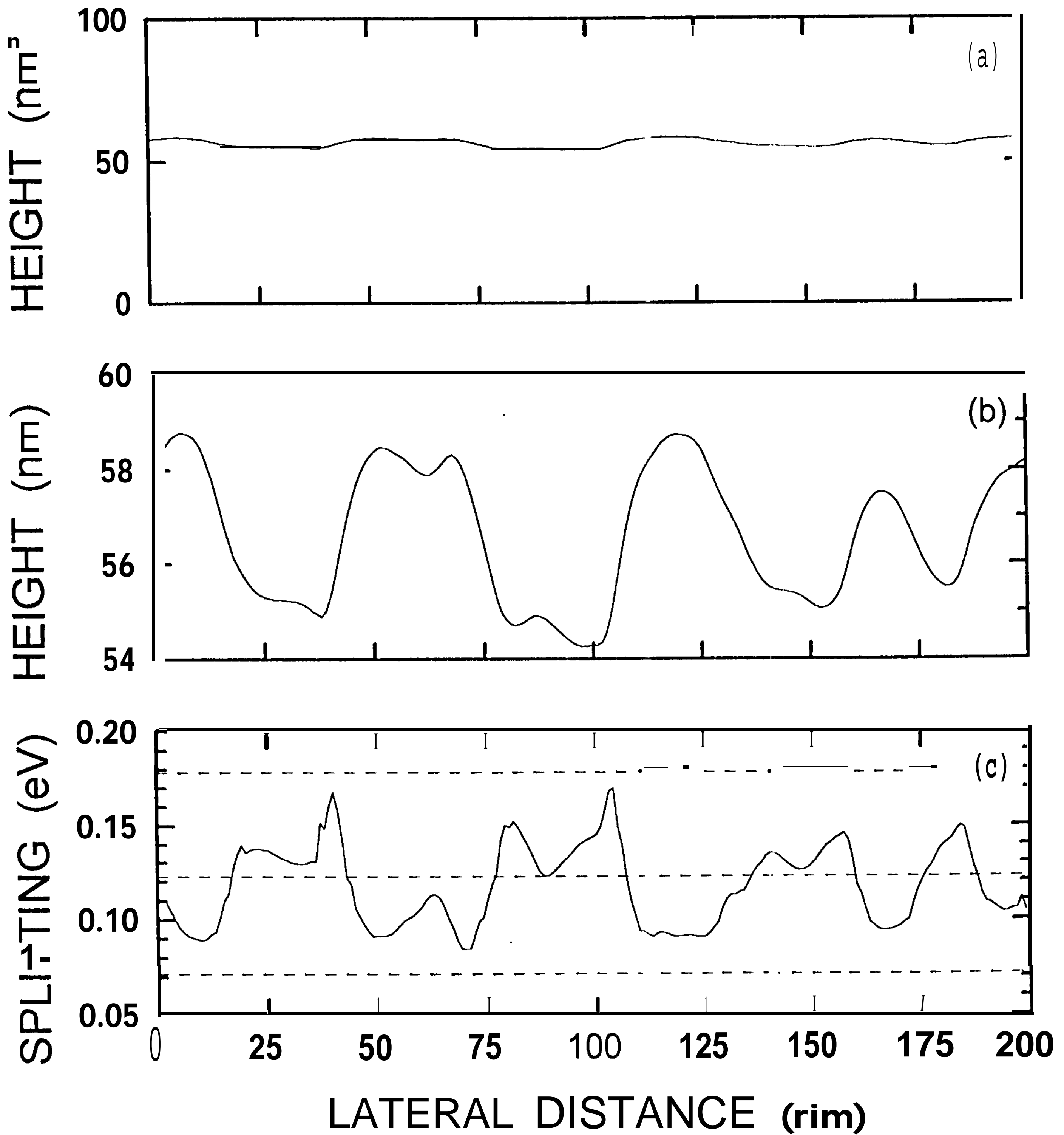

HEIGHT (nm)
100
50
0
(a)
HEIGHT (nm)
60
58
56
54
(b)
SPLI-TING (eV)
0.20
0.15
0.10
0.05
(c)
0
25
50
75
100
125
150
175
200
LATERAL DISTANCE (rim)

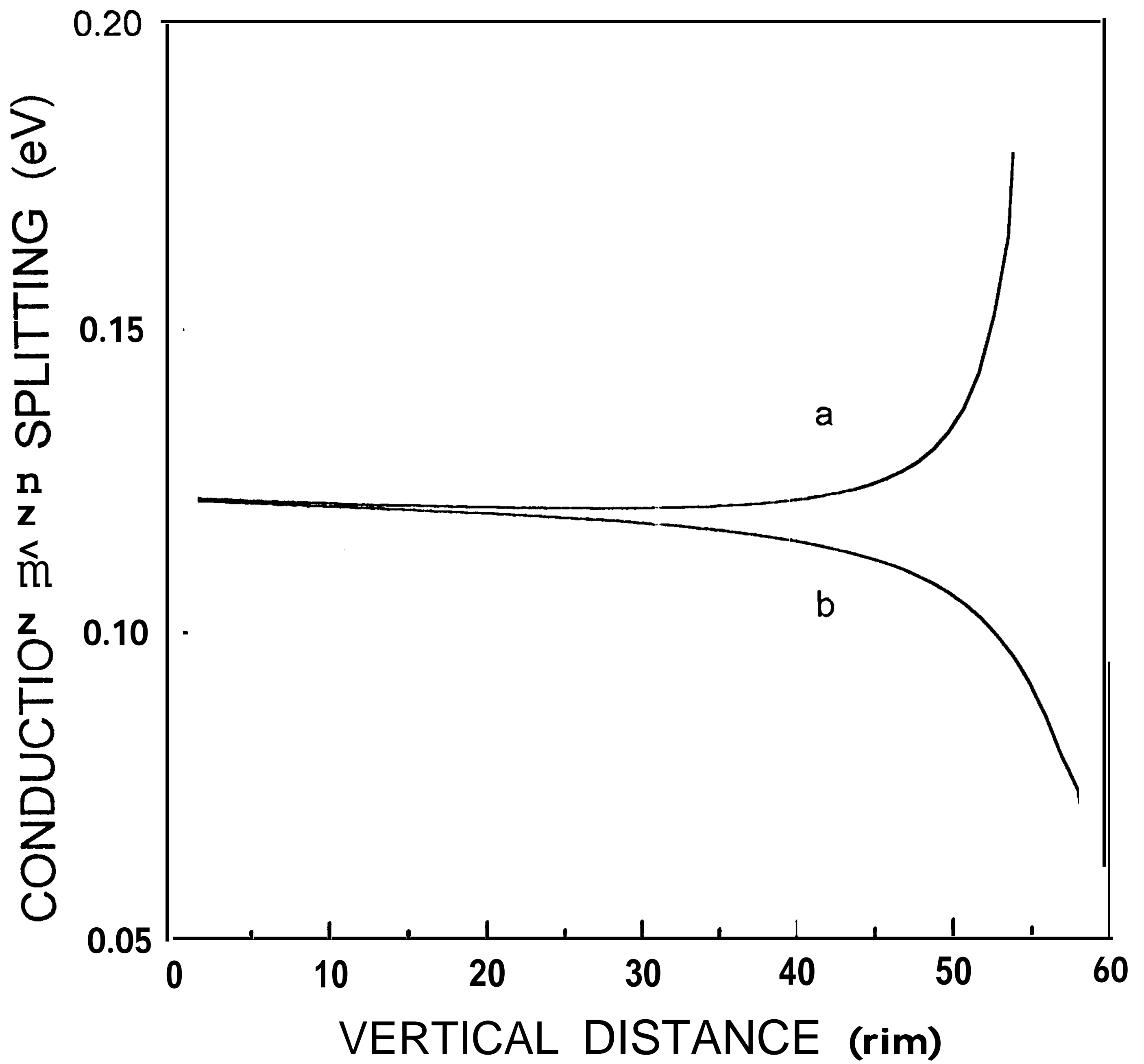

SiGe 16a
Exp.
corrected

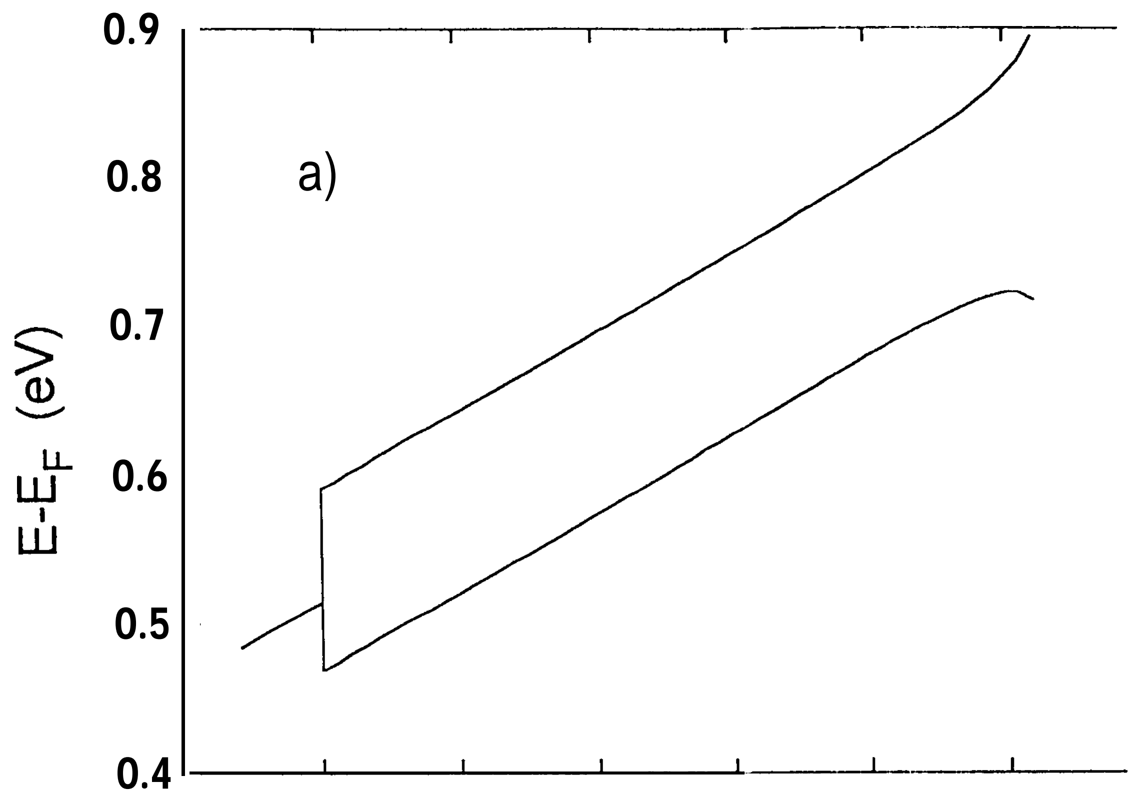

0.9
0.8
0.7
0.6
0.5
0.4
a)
E-E$_F$ (eV)

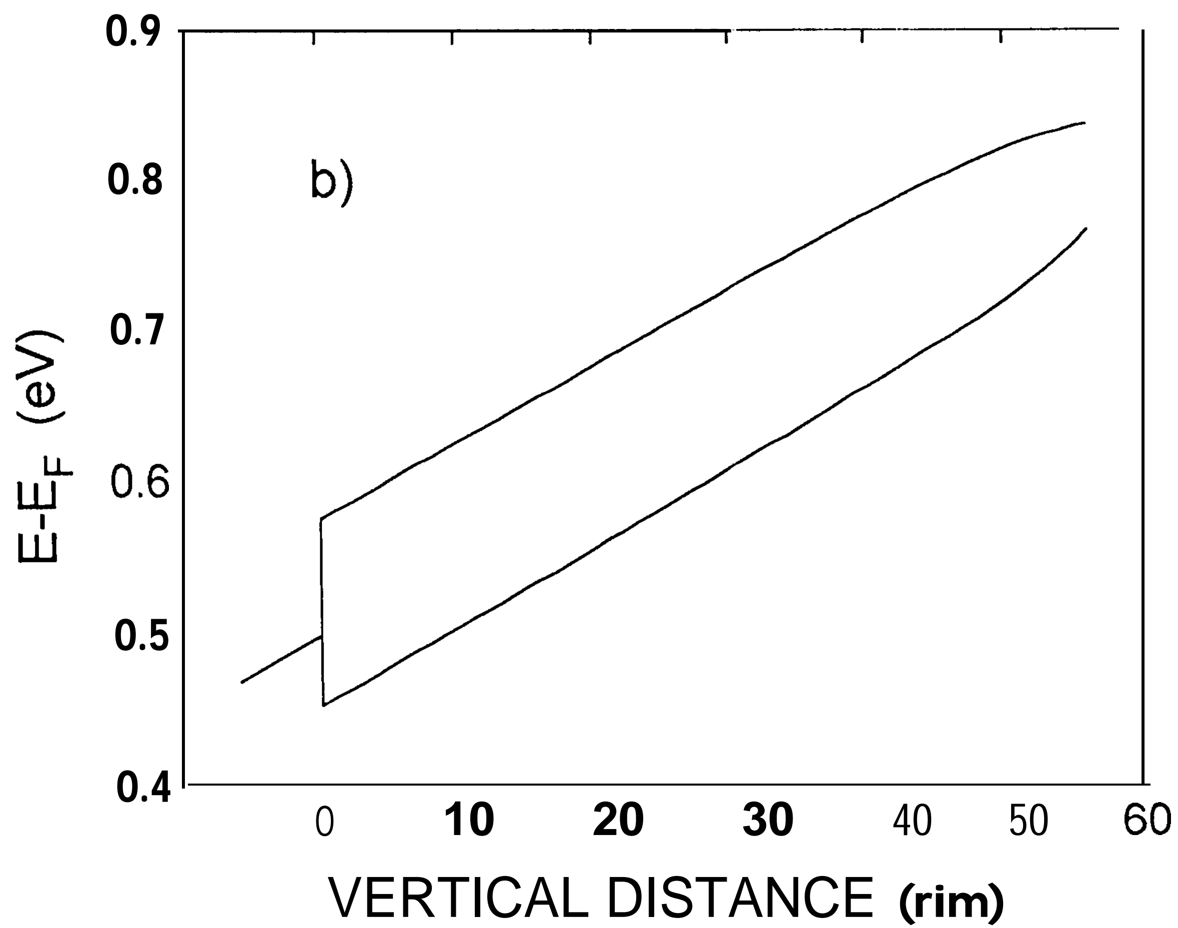

0.9
0.8
0.7
0.6
0.5
0.4
b)
E-E$_F$ (eV)
0
10
20
30
40
50
60
VERTICAL DISTANCE (rim)